

Strongly coupled semiconductor microcavities: A route to couple artificial atoms over micrometric distances

M. Benyoucef* and S. Kiravittaya

*Max-Planck-Institut für Festkörperforschung, Heisenbergstrasse 1, D-70569 Stuttgart, Germany*Y. F. Mei, A. Rastelli,[†] and O. G. Schmidt*Institute for Integrative Nanosciences, IFW Dresden, Helmholtzstrasse 20, D-01069 Dresden, Germany*

(Received 10 August 2007; published 8 January 2008)

We fabricate closely spaced microdisk resonators with embedded quantum dots (QDs) as emitters. By continuously tuning the refractive index of one of the microcavities, we observe clear molecularlike modes with “bonding” and “antibonding” characters, as confirmed by detailed finite-difference time-domain simulations. Based on recent reports on strong coupling between a single QD and a cavity mode, we propose to use modes in “photonic molecules” as a means to coherently transfer excitation between resonant QDs placed in different cavities.

DOI: [10.1103/PhysRevB.77.035108](https://doi.org/10.1103/PhysRevB.77.035108)

PACS number(s): 42.55.Sa, 78.55.Cr, 78.66.Fd, 78.67.Hc

I. INTRODUCTION

The creation of tailored matter composed of interacting quantum objects is attracting much interest, as it gives the chance to study quantum phenomena in controlled systems and opens up the opportunity for applications in the field of quantum information processing and communication. Semiconductor quantum dots (QDs), which confine charge carriers in all three directions, are promising candidates to build up controlled solid-state quantum systems. Much progress has been recently obtained in the field of QDs defined by split-gate techniques,¹ but the operation of such systems is limited to ultralow temperatures because of the weakly confining nature of the obtained QDs. Self-assembled QDs, on the other hand, have large confinement energies, and their manipulation and/or readout can be achieved by optical means. Two main routes are being investigated to achieve coupling between self-assembled QDs. The first relies on the fabrication of nearby (some nanometers apart) QDs (QD molecules), which can interact either by charge-carrier tunneling or by dipole-dipole interaction.^{2–6} The second relies on the use of light confined in a semiconductor microcavity to transfer excitation between QDs.⁷

One of the main obstacles toward the realization of both schemes is represented by the structural inhomogeneities inherent in the self-assembly approach, which reflect in differences in transition energies in the range of several tens of meV. An external electric field can be used to compensate for small inhomogeneities (meV), thus allowing the observation of coupling in QD molecules.^{2–6} The reduction of the dephasing time of the system produced by large fields⁸ will probably limit the applicability of such a method to a small number of QDs.

The recent demonstration of the quantum nature of the strong coupling between a QD exciton and a photon confined in a photonic crystal membrane cavity with high quality factor Q (Ref. 9) stimulates further research on strategies to couple QDs through cavity modes. Embedding energetically resonant QDs at well defined positions of the same microcavity is, however, a formidable technological challenge.

Furthermore, it would then be difficult to address them optically independently.

A possible solution to overcome these problems is to produce resonant but spatially separated QDs and use coupled optical microcavities to allow for excitation exchange among the QDs, as recently proposed in Ref. 10 for atoms. Using coupled cavities to mediate the interaction between QDs may have several advantages: (i) tuning the energy of spatially separated QDs is feasible,¹¹ (ii) the different QDs separated by some micrometers may be addressed individually, and (iii) the interaction may be switched on and off by detuning the QDs (e.g., by means of a local electric field) or the cavities (by refractive index tuning). For this kind of approach, it is important to study in detail the (classical) strong coupling between two nearby microcavities, also referred to as “photonic molecules” (PMs).¹²

When a PM consists of two or more closely spaced identical microcavities, coupling results in the formation of molecularlike modes with bonding and antibonding characters, similar to real molecules. This phenomenon has been demonstrated in square semiconductor microcavities coupled by a narrow channel,¹² in a dye-stained bisphere system,¹³ and in spherical microcavities.^{14,15} The mode splitting depends on the coupling efficiency, which in turn depends on the mode characteristics and distance between the resonators composing the PM.¹⁶ Different theoretical approaches have been developed to model the coupling of microcavities in PMs,^{16–19} mainly motivated by the application of PMs as passive (e.g., delay lines^{20,21}) or active (e.g., lasers²²) components in integrated photonic circuits. On the other hand, the experimental investigations of the coupling are rendered difficult by unavoidable structural fluctuations occurring in real systems.

In this paper, we fabricate PMs consisting of high quality closely spaced microdisks containing self-assembled QDs as emitters and investigate the coupling of whispering gallery modes (WGMs) in detail. In order to compensate small fluctuations in the mode positions, we use a focused laser beam both as optical excitation and local heat source. By locally heating one of the disks composing the PM, we controllably

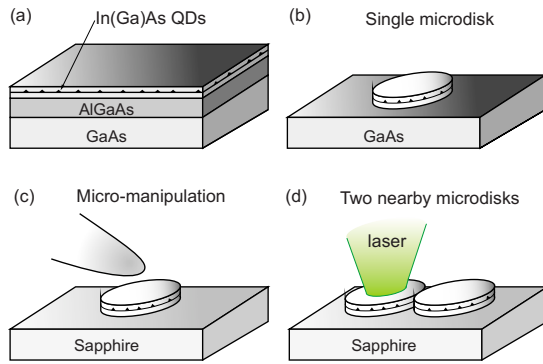


FIG. 1. (Color online) Schematic illustration of the fabrication and manipulation methods of GaAs microdisks containing In(Ga)As QDs.

increase its refractive index and consequently redshift the confined WGMs, without changing the intercavity coupling distance. When WGMs of two disks are brought into resonance, clear anticrossings are observed, which witness the strong coupling between the two resonators. Different energy splittings (i.e., coupling efficiencies) are observed for different modes. WGM calculations and two-dimensional (2D) finite-difference time-domain (FDTD) simulations allow us to classify the observed modes and to explain the different coupling efficiencies for different modes.

II. EXPERIMENT

The sample considered here was grown by solid-source molecular beam epitaxy on a semi-insulating GaAs(001) substrate. After standard deoxidation and buffer growth, a $1\ \mu\text{m}$ thick $\text{Al}_{0.7}\text{Ga}_{0.3}\text{As}$ sacrificial layer was deposited. The active structure consists of In(Ga)As QDs placed in the middle of a $200\ \text{nm}$ thick GaAs layer sandwiched between two $20\ \text{nm}$ thick $\text{Al}_{0.3}\text{Ga}_{0.7}\text{As}$ cladding layers and $10\ \text{nm}$ GaAs. The sample was then processed by electron beam lithography and a two-step wet chemical etching to obtain microdisks, as described in detail in Ref. 23. For the present experiment, microdisks were completely underetched [Fig. 1(b)] and micromanipulated under an optical microscope with a glass capillary to build up a PM on a sapphire substrate with low refractive index $n=1.77$ [Figs. 1(c) and 1(d)]. Different disks show slight fluctuations in the mode positions, due to unavoidable differences in the disk geometry and possibly to differences in the structure of the interface between the disk and the sapphire substrate.

For photoluminescence (PL) investigations, the sample was mounted in a cold-finger helium flow cryostat which can be moved by computer-controlled xy -linear translation stages for exact positioning with a spatial resolution of $50\ \text{nm}$. For the excitation of our sample structure, the laser beam (continuous wave, $532\ \text{nm}$ wavelength) passes a variable power attenuator and is focused by a microscope objective (with numerical aperture=0.6) to a spot diameter of $\sim 1.5\ \mu\text{m}$. The same microscope objective is used to collect the emission, which is then spectrally filtered by a $0.75\ \text{m}$ focal length spectrometer equipped with a liquid nitrogen cooled charge

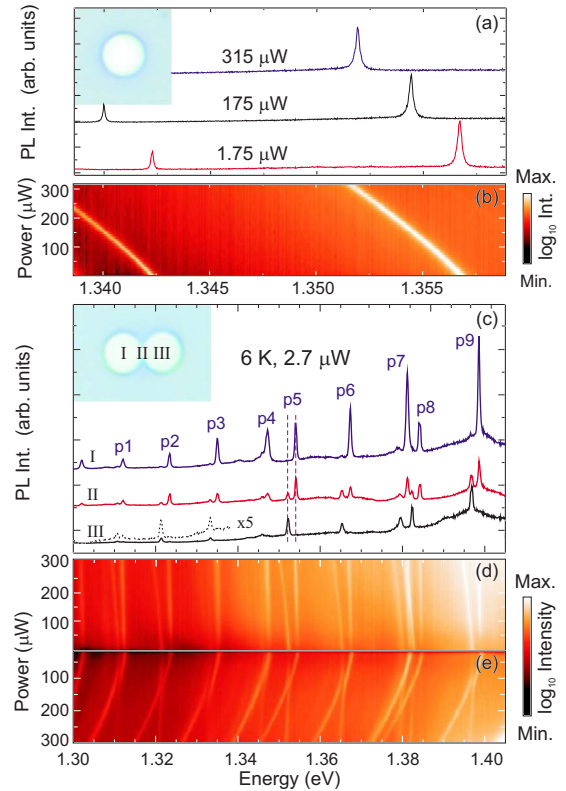


FIG. 2. (Color online) (a) Photoluminescence (PL) spectra of a single disk on sapphire substrate taken at three different laser powers. The inset is an optical microscopy image of a disk with diameter $D \sim 2.8\ \mu\text{m}$. (b) PL intensity map of a single disk as a function of emission energy and laser power. (c) Low resolution PL spectra extracted from a space map at low laser power ($2.7\ \mu\text{W}$) of two nearby disks for three different locations as indicated in the optical microscopy image shown in the inset. PL intensity maps with the laser beam centered on (d) the right disk (III) and (e) the left disk (I).

coupled device. No spatial filtering is used to limit the collection area. All the measurements are performed with the sapphire substrate at a temperature of $6\ \text{K}$.

III. RESULTS AND DISCUSSION

The relatively bad thermal contact between disks and the sapphire substrate allows us to use the laser beam both as excitation and heat source to tune their refractive index at relatively low laser powers. Figure 2(a) shows three high resolution PL spectra at different laser powers for a single disk with diameter $D \sim 2.8\ \mu\text{m}$ (see optical microscopy image in the inset). The spectra consist of two well separated sharp PL peaks with Q values $> 10\ 000$. By continuously increasing the laser power, we can smoothly increase the temperature (and hence the refractive index) of the disk. In turn, the refractive index increase produces a smooth shift of the modes toward longer wavelengths, as shown in the intensity map in Fig. 2(b). This simple tool allows us to compensate the size fluctuations of different disks and study the coupling properties of a PM in detail.

TABLE I. Mode identification [see top spectrum in Fig. 2(c)] and energy splittings of TE and TM modes at the resonance. Note that the energy splitting of p7 cannot be resolved because it is below the resolution of our PL setup.

Peak	Mode index	Energy splitting (meV)
p1	TE(1,24)	1.2
p2	TE(2,20)	0.8
p3	TM(1,23)	1.4
p4	TE(1,25)	0.8
p5	TE(2,21)	0.7
p6	TM(1,24)	1.2
p7	TE(1,26)	
p8	TE(2,22)	0.5
p9	TM(1,25)	1.0

Figure 2(c) displays low resolution PL spectra extracted from a space map at low laser power ($2.7 \mu\text{W}$) of two closely spaced disks for three different locations (indicated in the optical microscopy image in the inset). The separation between the two disks is well below the resolution of our optical microscope. The top and bottom spectra are taken by focusing the laser on top of the left disk (I) and right disk (III), respectively. The well separated sharp lines in the PL spectra correspond to different transverse electric (TE) and transverse magnetic (TM) modes (see below). Apart from a slight shift ($\sim 3 \text{ meV}$) of the mode positions, the two spectra show very similar features. We therefore assign the mode shifts to a slight difference in disk diameter with the left disk having smaller D compared to the right disk. The middle spectrum (II) is taken by focusing the laser on the contact point of the two disks and shows the modes of both disks. TE and TM WGMs in microdisks can be classified according to their radial mode number l and azimuthal mode number m and will be denoted in the following as TE/TM(l, m). Using the whispering gallery mode approximation,²⁴ we identify the peaks (p1–p9), as shown in Table I. [We define the “wave propagation” axis z as the direction perpendicular to the substrate. TE (TM) modes are characterized by the electric field F (magnetic field H) perpendicular to such axis].

We first focus the laser beam on top of the “larger” disk and increase the laser power gradually (changing the refractive index). The modes of both disks redshift but the modes of the larger disk shift at a higher rate, resulting in a gradual separation of the modes [see Fig. 2(d)]. We now place the laser beam on the center of the “smaller” disk and heat it in a similar way. In contrast to the results shown in Fig. 2(d), for certain values of the power, the modes of the two disks are brought into resonance and clear anticrossing patterns emerge for all pairs of modes [Fig. 2(e)]. This observation demonstrates that the two disks represent a PM and that molecularlike WGMs form when the modes of the two disks are brought into resonance.

In order to understand the coupling behavior, high resolution PL measurements are performed with the laser focused on the “small” disk. As an example, we have chosen peaks

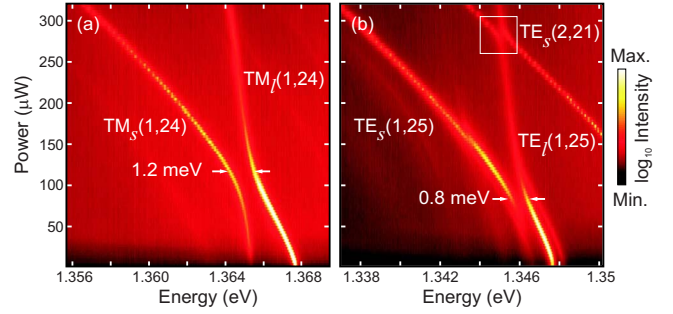


FIG. 3. (Color online) High resolution PL intensity maps as a function of laser power (corresponding to change in the refractive index of the “small” disk) and emission energy for (a) TM(1,24) and (b) TE(1,25).

p4 and p6, corresponding to TE and TM, respectively. Figures 3(a) and 3(b) display high resolution PL spectra as a function of laser power. In both cases, the two modes first approach and then separate when the power is increased, showing clean anticrossing characteristics. The energy splitting values are 1.2 and 0.8 meV for TM(1,24) and TE(1,25), respectively, which are larger than the linewidth of the individual modes ($\sim 0.25 \text{ meV}$). This is an evidence of strong coupling of WGMs in the PM. By further increasing the laser power, we observe a second anticrossing between the first-order radial mode of the “large” disk $\text{TE}_l(1,25)$ and a second-order radial mode of the “smaller” disk $\text{TE}_s(2,21)$ [see Fig. 3(b)]. The energy splittings for the other modes are listed in the second column of Table I. These examples illustrate how the simple refractive index tuning used here allows the detailed study of the coupling efficiency of different modes “in one shot.”

To explain the coupling characteristics and the differences in energy splittings, we performed 2D FDTD simulations for the PM considered here. First, the effective refractive index (n_{eff}) for each TE and TM mode is calculated from the vertical structure.²⁵ From the optical microscopy image [see the inset of Fig. 2(c)], we obtain disk diameters of $\sim 2.8 \mu\text{m}$. Since from the PL spectra a redshift of $\sim 3 \text{ meV}$ is measured for all modes of the right disk compared to the left disk, we estimate the difference in diameter of both disks to be $\sim 3 \text{ nm}$. The energy separation between the molecular modes at the resonance between two interacting WGMs is expected to critically depend on the distance between the two disks.¹⁸ Since we have no experimental access to this quantity, in the simulation, we have treated it as an adjustable parameter. A value of 70 nm was chosen to obtain energy splitting values close to the experimentally observed values. We concentrate on the representative modes TM(1,24) and TE(1,25) shown in Fig. 3 to make a direct comparison to the experimental data. In the FDTD calculation, the effective refractive index of the smaller disk $n_{eff}^s(E)$ is varied as a function of temperature, while the refractive index of the larger disk $n_{eff}^l(E)$ is kept constant to the value calculated at 6 K. The temperature dependence of $n(E)$ for GaAs is taken from Ref. 26 and used to calculate the temperature dependence of $n_{eff}^s(E)$.

The simulated spectra and the corresponding electric F and magnetic H field profiles of the two modes are shown in

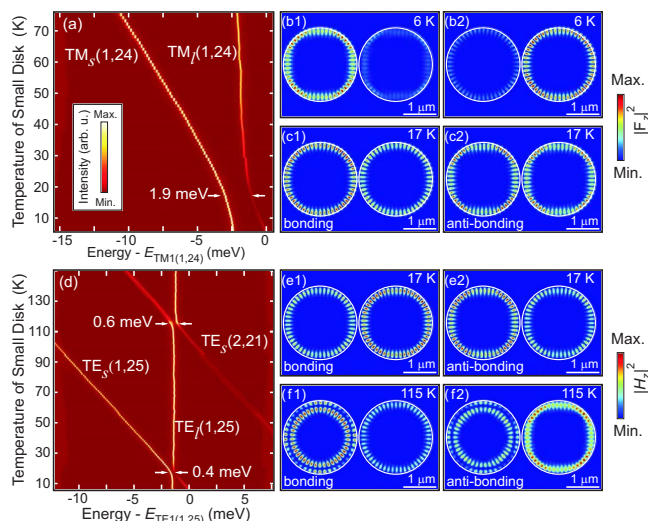


FIG. 4. (Color online) Simulated PL spectra as a function of temperature for (a) TM(1,24) and (d) TE(1,25). Calculated magnetic fields: (b1) and (b2) when the disks are not in resonance (the disk diameter is slightly different) and (c1) and (c2) when the disks are in resonance. Calculated electric fields: (e1) and (e2) when the disks are in resonance and (f1) and (f2) for higher order mode.

Fig. 4. By changing $n_{eff}(E)$ (corresponding to heating the smaller disk), anticrossings are clearly visible and comparable to the experimental data. The simulated energy splitting values are 1.9 and 0.4 meV for TM(1,24) and TE(1,25), respectively. The discrepancy with the experiment might be due to the imperfection of the disks and also to the effect of neglecting the sapphire substrate in the simulation. From the experiment and the simulation, the TM modes generally show larger energy splittings compared to the TE modes (see Table I). The simulation suggests that this is due to the TM modes having larger field intensity close to the disk edge. Using this simulation, we also reproduced a similar anti-

crossing of a higher-order radial mode $TE_s(2,21)$ with the first-order radial mode $TE_s(1,25)$ as found in the experiment. When the disks are not in resonance (same temperature but different size), the modes are localized in separate disks [Figs. 4(b1) and 4(b2)]. When the disks are in resonance (the slight difference in the disk diameter is compensated by the change of refractive index of the small disk), the modes spread over the two disks and show bonding and antibonding characters [Figs. 4(c1)–4(f2)].

IV. CONCLUSIONS AND PERSPECTIVES

In conclusion, we have fabricated PMs consisting of two adjacent GaAs microdisks on a sapphire substrate and we have studied in detail the formation of molecularlike modes by tuning the refractive index of the smaller disk using a slow and selective heating process. Whispering gallery mode calculations and finite-difference time-domain simulations allowed us to rationalize the experimental results. While we have considered here a photonic molecule consisting of relatively large microdisks with high density of randomly arranged QDs, we envision the possibility of using similar systems to mediate coherent interaction between two or more QDs. A viable path consists in (i) placing QDs at well defined positions of a substrate by, e.g., growth on prepatterned substrates,²⁷ (ii) use the *in situ* laser processing to tune a number of QDs into resonance with each other,¹¹ and (iii) fabricate coupled microcavities with smaller mode volumes and geometry to have modes matching the QD emission and with position such that the QDs are located at the field maxima.^{9,28}

ACKNOWLEDGMENTS

This work was financially supported by the BMBF (01BM459) and DFG (Research group: *Positioning of single nanostructures-single quantum devices*).

*Present address: Institute for Integrative Nanosciences, IFW Dresden, Helmholtzstrasse 20, D-01069 Dresden, Germany. m.benyoucef@ifw-dresden.de

†a.rastelli@ifw-dresden.de

¹F. H. L. Koppens, C. Buizert, K. J. Tielrooij, I. T. Vink, K. C. Nowack, T. Meunier, L. P. Kouwenhoven, and L. M. K. Vander-sypen, *Nature (London)* **442**, 766 (2006).

²G. Ortner, M. Bayer, Y. Lyanda-Geller, T. L. Reinecke, A. Kress, J. P. Reithmaier, and A. Forchel, *Phys. Rev. Lett.* **94**, 157401 (2005).

³H. J. Krenner, M. Sabathil, E. C. Clark, A. Kress, D. Schuh, M. Bichler, G. Abstreiter, and J. J. Finley, *Phys. Rev. Lett.* **94**, 057402 (2005).

⁴G. J. Beirne, C. Hermannstädter, L. Wang, A. Rastelli, O. G. Schmidt, and P. Michler, *Phys. Rev. Lett.* **96**, 137401 (2006).

⁵A. Stinaff, M. Scheibner, A. S. Bracker, I. V. Ponomarev, V. L. Korenev, M. E. Ware, M. F. Doty, T. L. Reinecke, and D. Gammon, *Science* **311**, 636 (2006).

⁶L. Wang, A. Rastelli, S. Kiravittaya, M. Benyoucef, and O. G. Schmidt, arXiv:cond-mat/0612701 (unpublished).

⁷A. Imamoğlu, D. D. Awschalom, G. Burkard, D. P. DiVincenzo, D. Loss, M. Sherwin, and A. Small, *Phys. Rev. Lett.* **83**, 4204 (1999).

⁸S. Stuffer, P. Ester, A. Zrenner and M. Bichler, *Phys. Rev. Lett.* **96**, 037402 (2006).

⁹K. Hennessy, A. Badolato, M. Winger, D. Gerace, M. Atatüre, S. Gulde, S. Fält, E. L. Hu, and A. Imamoğlu, *Nat. Phys.* **445**, 896 (2007).

¹⁰M. J. Hartmann, F. G. S. L. Brandao, and M. B. Plenio, *Nat. Phys.* **2**, 849855 (2006).

¹¹A. Rastelli, A. Ulhaq, S. Kiravittaya, L. Wang, A. Zrenner, and O. G. Schmidt, *Appl. Phys. Lett.* **90**, 073120 (2007).

¹²M. Bayer, T. Gutbrod, J. P. Reithmaier, A. Forchel, T. L. Reinecke, P. A. Knipp, A. A. Dremin, and V. D. Kulakovskii, *Phys. Rev. Lett.* **81**, 2582 (1998).

¹³T. Mukaiyama, K. Takeda, H. Miyazaki, Y. Jimba, and M.

- Kuwata-Gonokami, Phys. Rev. Lett. **82**, 4623 (1999).
- ¹⁴Y. P. Rakovich, J. F. Donegan, M. Gerlach, A. L. Bradley, T. M. Connolly, J. J. Boland, N. Gaponik, and A. Rogach, Phys. Rev. A **70**, 051801(R) (2004).
- ¹⁵B. M. Möller, U. Woggon, M. V. Artemyev, and R. Wannemacher, Phys. Rev. B **70**, 115323 (2004).
- ¹⁶A. V. Kanaev, V. N. Astratov, and W. Cai, Appl. Phys. Lett. **88**, 111111 (2006).
- ¹⁷S. Deng, W. Cai, and A. V. Kanaev, Opt. Express **12**, 6468 (2004).
- ¹⁸J.-W. Ryu, S.-Y. Lee, C.-M. Kim, and Y.-J. Park, Phys. Rev. A **74**, 013804 (2006).
- ¹⁹S. Boriskina, Opt. Lett. **31**, 338 (2006).
- ²⁰J. E. Heebner and R. W. Boyd, J. Mod. Opt. **49**, 2629 (2002).
- ²¹Y. Hara, T. Mukaiyama, K. Takeda, and M. Kuwata-Gonokami, Phys. Rev. Lett. **94**, 203905 (2005).
- ²²A. Nakagawa, S. Ishii, and T. Baba, Appl. Phys. Lett. **86**, 041112 (2005).
- ²³A. Rastelli, A. Ulhaq, Ch. Deneke, L. Wang, M. Benyoucef, E. Coric, W. Winter, S. Mendach, F. Horton, F. Cavallo, T. Merdzhanova, S. Kiravittaya, and O. G. Schmidt, Phys. Status Solidi C **3**, 3641 (2006).
- ²⁴See, e.g., N. C. Frateschi and A. F. J. Levi, J. Appl. Phys. **80**, 644 (1996).
- ²⁵P. Yeh, *Optical Waves in Layered Media* (Wiley, Hoboken, NJ, 2005), p. 305.
- ²⁶*Properties of Gallium Arsenide*, EMIS Datareviews Series, 3rd ed., edited by M. R. Brozel and G. E. Stillman (INSPEC, London, 1996).
- ²⁷S. Kiravittaya, M. Benyoucef, R. Zapf-Gottwick, A. Rastelli, and O. G. Schmidt, Appl. Phys. Lett. **89**, 233102 (2006).
- ²⁸A. Badolato, K. Hennessy, M. Atatüre, J. Dreiser, P. M. Petroff, and A. Imamoglu, Science **308**, 1158 (2005).